Available online at www.sciencedirect.com
ScienceDirect
Trans. Nonferrous Met. Soc. China 21(2011) 1925−1931
Transactions of Nonferrous Metals Society of China
www.tnmsc.cn

Mechanical properties and wear resistance of aluminum composite welded by electron beam

PENG Kun, CUI Hai-chao, LU Feng-gui, WU Xiao-min, TANG Xin-hua, YAO Shun, LOU Song-nian

Shanghai Key Laboratory of Materials Laser Processing and Modification,
Shanghai Jiao Tong University, Shanghai 200240, China

Received 17 June 2010; accepted 15 August 2010

Abstract: The welding property of TiB_2/ZL101 composite was investigated using electron beam (EB) welding experimental system with a function generator. The fine defect-free welding seam was obtained under proper processing parameters and scanning rate. The reinforcement particles TiB_2 distributed homogeneously in welding seam without any segregation. The tensile results show that fracture occurs at the base metal and elastic modulus increases compared with base metal. Wear resistance of welding seam is improved greatly compared with base metal. The results show that the TiB_2/ZL101 composite can be successfully welded by EB technology.

Key words: TiB_2/ZL101composite; electron beam welding; segregation; tension; wear resistance

1 Introduction

In situ TiB_2/ZL101 composite is a kind of new structure-functional material which has been used in the military and semiconductor industry. Compared with SiC often chosen as reinforcement, TiB_2 particles have many advantages such as higher melting point, higher hardness and higher elastic modulus, and also much better surface wetting ability with aluminum than that of SiC [1]. But the weldability of this kind of new material has not been deeply studied. Currently the most common welding methods for aluminum matrix composites mainly include arc welding, capacitor discharge welding, laser welding, diffusion welding, brazing and friction welding. But it is very difficult to get the fine defect-free welding seam due to porosity and particle segregation, and there is also a great interface reaction tendency for reinforcement during the welding process [2−4]. LI et al [5] made a deep study on weld ability of SiC_p reinforced Al-matrix composite by arc welding and found that the interface reaction could not be prevented. However, GARCIA et al[6] carried out metal inert gas welding (MIG) of Al 1010/TiC/50_p composites by applying the electric arc indirectly, and the dissolution of reinforcement was successfully controlled and Al_4C_3 was not detected. LI et al [7] carried out the experiment of welding A356Al/TiB_2 using friction stir welding (FSW) and found that the welding quality was very sensitive to FSW parameters. LIU et al [8] studied the laser welding Al_2O_{3p}/6061 Al composites and found that segregation of Al_2O_3 was also present due to the great difference between ceramics and aluminum matrix. NIU et al [9] made deep study on Al_2O_{3p}/6061 Al by diffusion welding (DFW) and found that the key parameter affecting joint strength is welding temperature. Electron beam (EB) welding has been improved to be an flexible method to aluminum matrix composites by CUI et al [10] and some exciting results were obtained. But the further mechanical properties have not been studied and reported yet. Also, JI et al [11] discussed the problems in EB welding of SiC particulate reinforced aluminum composite.

How to obtain the defect-free welding seam by optimal EB parameters will be discussed in this work and research on the joint mechanical properties including tensile property and wear resistance will be carried out. The qualified welding performance of this new material will be helpful to expand its application.

2 Experimental

In situ TiB_2/ ZL101 composite (14% TiB_2, mass fraction) was employed, which was supplied by Institute of Ecology and Environmental Materials of Shanghai

Foundation item: Project (11ZR1417500) supported by Natural Science Foundation of Shanghai, China
Corresponding author: LU Feng-gui; Tel: +86-21-54748940-8025; E-mail: lfg119@sjtu.edu.cn
DOI: 10.1016/S1003-6326(11)60951-5

Jiao Tong University, China. The chemical compositions of TiB_2/ZL101 are shown in Table 1. The microstructure of this aluminum matrix composite material is presented in Fig. 1. The nanometer-sized TiB_2 particles cluster together and the mean cluster size changes from 2 to 100 μm.

Table 1 Chemical compositions of TiB_2/ZL101 (mass fraction, %)

Si	Mg	Zr	Fe	Al
6.67	0.45	0.42	0.14	Bal.

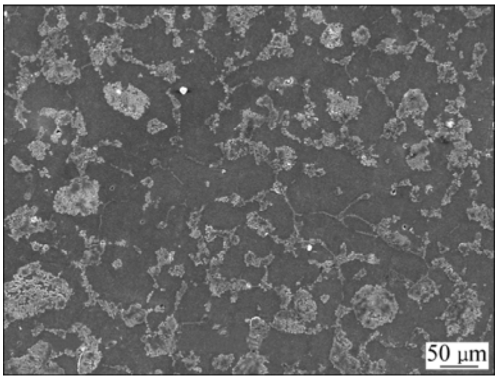

Fig. 1 Microstructure of TiB_2/ZL101 composite

All welding experiments were carried out on a EBW−6C model electron beam welding machine, and the scanning circular heat source with a certain frequency was applied to the surface of composite plate. The size of experimental plate used in EB welding was 8 mm in thickness, 100 mm in length and 50 mm in width. The pieces were cleaned carefully with acetone thoroughly to eliminate dirt and grease before welding. Microstructures of the polished metallographic cross-sections were observed by SEM. Tensile tests were carried out at room temperature on a universal testing machine. The degree of vacuum in EBW was 7.0×10^{-2} Pa. The dry-sliding wear tests were carried out on a universal wear resistance machine. The section of weld beam along the welding direction was taken as wear surface with 7 mm in length and 7 mm in width.

3 Results and discussion

3.1 Cross-section appearance of EB welds made at different heat inputs

Table 2 shows some welding parameters used in this experiment. Cross-section and surface appearance of EB welds made at different heat inputs is shown in Fig. 2, and the typical ‘nail’ welding seams can be observed. The higher the heat input is, the deeper and wider the beads are. The full penetration of the plate just occurs under EB power of 2 340 W (sample 3), as shown in Figs. 2 (c) and (d). In the tests, all the depth-to-width ratios were above 2.5, and heat affected zone (HAZ) was very narrow because beam diameter of the EB was only 0.1 mm. When the power was increased to 2.8 kW, the excessive penetration occurs, as shown in Figs. 2(e) and (f). Figure 3 shows the cross-section and surface appearance of welding at power of 2 340 W, the porosity is not observed in the bead.

When the EB impacted the surface metal, vaporization occurred and then the keyhole formed. The keyhole was depressed by the metal steam reaction force (F_a) and the EB pressure (F_e) while the σ and the hydrostatic pressure (F_d) played an opposite role. The basic equation relating F_a, F_e, σ and F_d can be obtained:

$$F_a + F_e \geq \sigma + F_d \tag{1}$$

In fact, F_a can be 10^4–10^5 times F_e, so the F_a plays a much more important role in deepening the keyhole compared with others. This means that the depth of keyhole increases as the heat input gradually increases. By the way, the heat conduction in vertical direction along the keyhole by metal vapor is much easier than that in horizontal direction by solid metal. In this study, the thermal conductivity of this aluminum matrix composite in horizontal direction further reduced after adding TiB_2 particles. The thermal conductivity of this composite can be calculated by Maxwell model [12]:

$$\lambda_{\mathrm{eff}} = \lambda_{\mathrm{m}} \left[\frac{2(\lambda_{\mathrm{p}} - \lambda_{\mathrm{m}})V_{\mathrm{p}} + \lambda_{\mathrm{p}} + 2\lambda_{\mathrm{m}}}{(\lambda_{\mathrm{m}} - \lambda_{\mathrm{p}})V_{\mathrm{p}} + \lambda_{\mathrm{p}} + 2\lambda_{\mathrm{m}}} \right] \tag{2}$$

Table 2 Process parameters of EB welding

Weld No.	Accelerating voltage/kV	Beam current/mA	Welding speed/ ($mm\cdot s^{-1}$)	Scanning frequency/Hz	Heat input/ ($J\cdot min^{-1}$)	Depth-to-width ratio
1	60	28	20	–	84	3.05
2	60	35	20	–	105	2.90
3	60	39	20	–	117	2.75
4	60	47	20	–	141	2.51
5	60	39	20	600	117	3.68
6	60	39	20	900	117	3.30

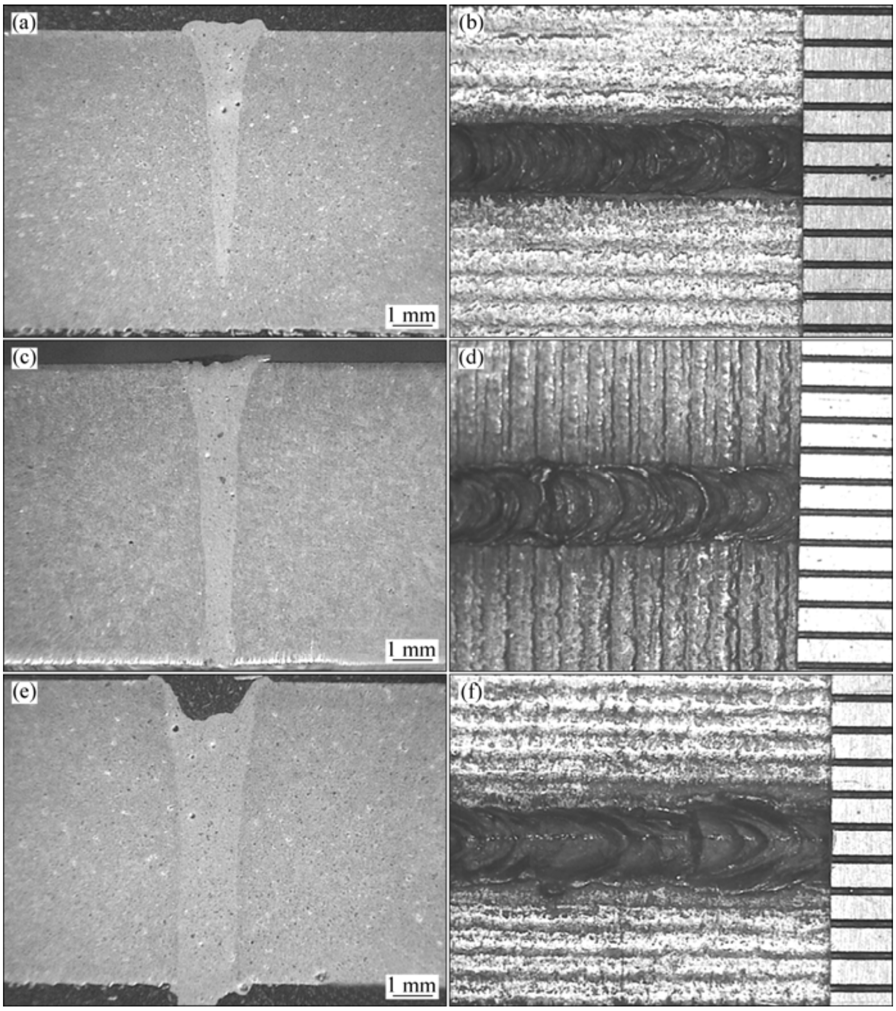

Fig. 2 Cross-section and surface appearance of welding seams under different EB process parameters: (a), (b) Sample 1; (c), (d) Sample 3; (e), (f) Sample 4

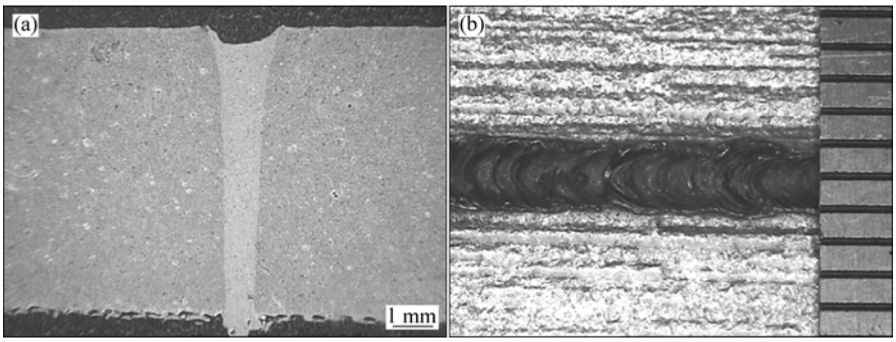

Fig. 3 Cross-section (a) and surface (b) appearance of sample 5

where λ_{eff} is the thermal conductivity of this composite; λ_m is the thermal conductivity of base metal; λ_p is the conductivity of TiB_2 particle; and V_p is the volume fraction of TiB_2 particles in the composite. The result shows that when TiB_2 particles (w=14%) are added, the thermal conductivity drops to only about 80% of the original conductivity. When the heat input increases, the depth of the bead becomes greater in the vertical direction while the width of the bead slightly changes.

Porosity can be observed close to fusion line (FL) at different degrees, confirming that most of the small pores may be hydrogen porosity [13]. The defect of porosity is mainly due to significantly different hydrogen solubilities for aluminum in the solid and liquid during welding process. The long-narrow weld seam is favorable for reducing the HAZ while it is also unfavorable for gas escaping in the bead. With proper process parameters and certain frequency scanning waveform, welding defects and porosity could be prevented successfully. This is because the scanning waveform makes the temperature distribution more homogeneous, in other words, the solidification rate decreases; at the same time, the flow of melt pool becomes much more violent due to the EB stirring effect. Both of the above facts are favorable for pores escaping from the bead. HALLUM and BAESLACK [14] carried out the similar experiment and also confirmed this point.

3.2 Refinement of matrix metal and dispersion of TiB_2 particles

Figure 4 shows the refinement of the matrix metal and the dispersion of TiB_2 particles in the base metal and the bead respectively. Not only is the grain of matrix metal in the base metal much larger than that of the bead, but also TiB_2 prior to welding is presented as larger clusters (diameter ≥20 μm) in the base metal while the clusters are separated (diameter ≤100 nm) after welding in the bead.

The matrix metal is well refined after welding. This is mainly because the nucleation rate (I) increases in the solidification process, which can be calculated by the following equation [15]:

$$I = N_1 v_0 pkn_s^* \exp(-\frac{\Delta G_n^* + \Delta G_d}{kT}) \quad (3)$$

where N_1 is the number of liquid atoms; v_0 is the atomic vibration frequency; p is the probability factor; k is the proportional coefficient; n_s^* is the possible position number for atoms on critical grain surface; ΔG_n^* is the variation of Gibbs free energy; ΔG_d is variation of active free energy; T is the temperature. As we know, the solidification rate of EB welding process is very high and the under-cooling to liquid metal could be great enough to decrease the nucleation energy. As previously mentioned in Eq. (3), the nucleation rate I will increase significantly so the matrix metal grows into fine equiaxed grains after EB welding. The refinement of matrix metal will have a great influence on the mechanical property of welding seam.

At the same time, the TiB_2 particles are also refined and separated. The key-hole moves along with the welding direction, and then the metal vapor erupts upward, which has a great impact on the back wall of the key-hole. The metal vapor stirs the melt pool forcefully to separate the TiB_2 clusters. In the fast solidification process many new nuclei appear, and then the matrix metal grows into fine equiaxed grains. The separated TiB_2 particles contract with much more α(Al) grains than before. When the α(Al) grains grow up, forces in all directions will be applied to the TiB_2 particles. If the lattice relationship between TiB_2 and Al is not met [16], the TiB_2 will be pushed rather than engulfed by solidification front during the process, so the TiB_2 particles distribute more homogeneously than before. The segregation of TiB_2 is prevented successfully. In conclusion, EB welding can effectively refine the welded metal microstructure under optimal parameters. ZHAO et al [17] proved this point. The study on the TiB_2 particle distribution provides encouraging evidence for the analysis of mechanical property improvement.

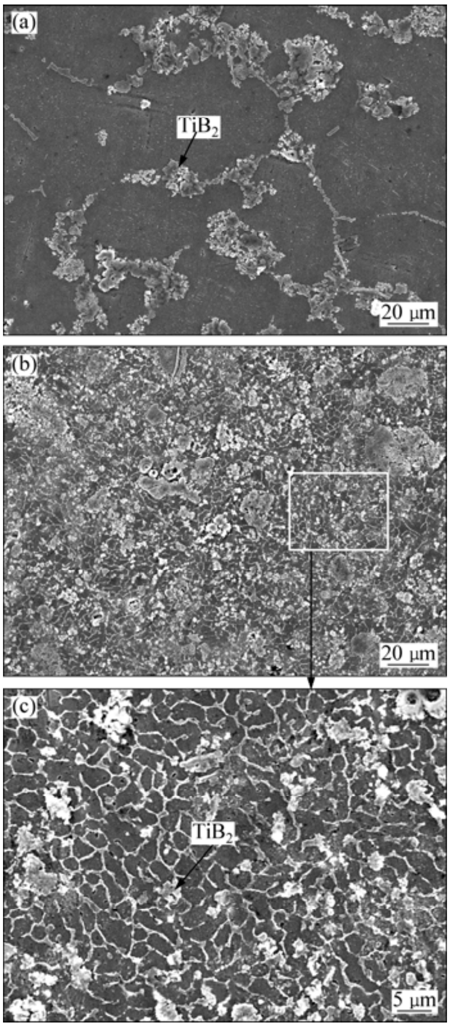

Fig. 4 Microstructures of sample 6: (a) Base metal; (b), (c) Welding seam

3.3 Tensile properties

The appearance of the fracture is shown in Fig. 5. It can be found that all fractures occur in the base metal, and the tensile strength for welded joint, which equals that of base metal, is 199.31 MPa (average value of three measurements). Figure 6 shows the stress—strain curves for this tensile test; the value of elastic modulus is 59.9 GPa which is about 110% of base metal. Compared with the base metal, samples 3 and 6 show higher elastic modulus due to the mechanical properties improvement in the welding seam.

Mechanical properties are determined by the microstructure of welding seam. The enhancement of tensile strength can be attributed to two aspects: fine grain strengthening and Orowan strengthening [18]. The mechanism will be explained respectively. Firstly, the matrix metal grows into fine equiaxed grains in the solidification process, so the grain boundaries increase greatly. The grain boundaries hinder the dislocations to pass by, and then the tensile strength correspondingly increases. Secondly, as previously mentioned, the reinforcement particles of TiB_2 were separated and distributed uniformly after welding. The spacing (λ) between TiB_2 particles is small enough. The equation relating intensity variation $\Delta\sigma_{or}$ and λ can be calculated by the following equation:

$$\Delta\sigma_{or}=2G\boldsymbol{b}/\lambda \tag{4}$$

where G is the shear modulus; $\boldsymbol{b}$ is the Burgers vector.

So the tensile strength is greatly improved according to the refinement of TiB_2 grain. Due to the fine grains, the stress in the bead distributes homogeneously. Once the stress concentration is significantly prevented, the initiation and propagation of cracks have been successfully delayed. So these welds show greatly high elastic modulus in the tests.

3.4 Dry-sliding wear resistance

The dry-sliding wear tests were carried out at room temperature. SEM micrographs of worn surface of both the base metal and the EB welding seam are shown in Fig. 7. Craters and deep grooves could be observed for

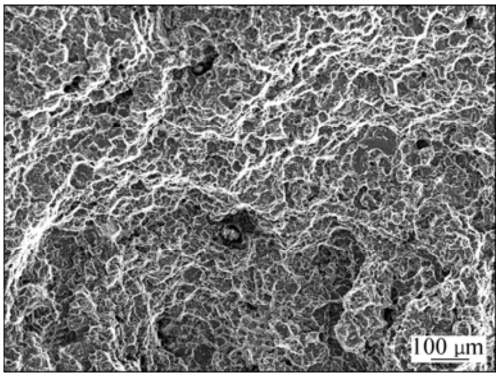

Fig. 5 SEM image showing fracture appearance for tensile test

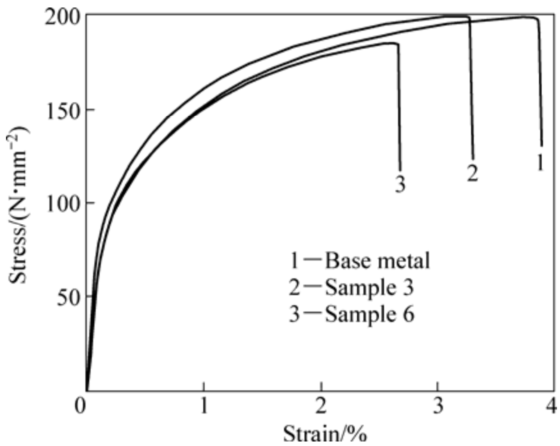

Fig. 6 Stress—strain curves of tensile test

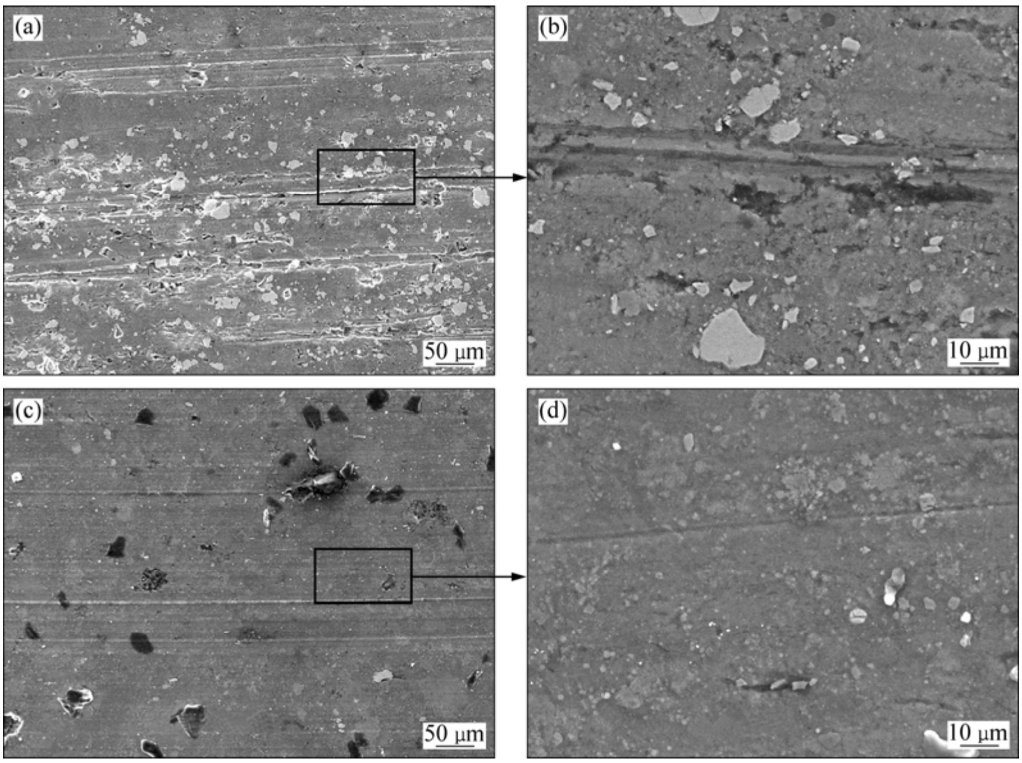

Fig. 7 SEM images of worn surface of EB joint: (a), (b) Base metal; (c), (d) Welding seam

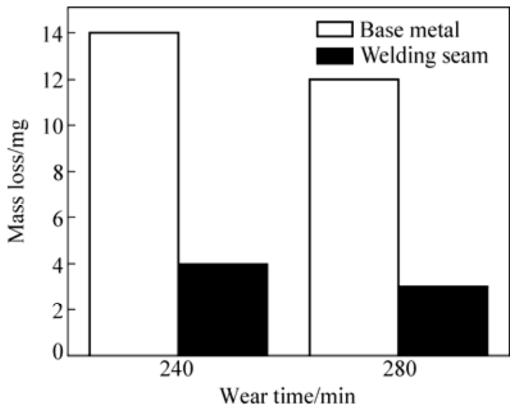

Fig. 8 Cumulative mass loss over 240 min during dry-sliding wear test

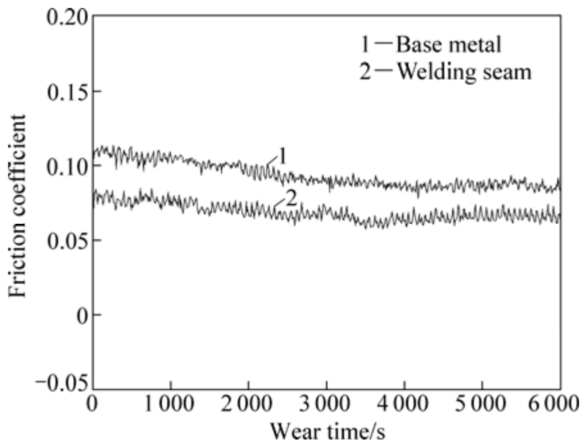

Fig. 9 Friction coefficient as function of wear time for base metal and welding seam

the base metal; however, the appearance seems rather smooth for the welding seam except some slight scratches. Figure 8 shows the cumulative mass loss over a period of 240 min during dry-sliding wear tests, the mass loss in base metal is 3 times that of welding seam. Figure 9 shows the variation of friction coefficient during the tests which is to be about 0.100 for the base metal and 0.075 for the welding seam. Both of the friction coefficients vibrate slightly with time.

The results illustrate that the dry-sliding wear resistance is greatly increased after EB welding. TiB_2 particles play an important role in resisting wear attacks. The dominant wear mechanism in the tests can be regarded as a refinement and reinforcement mechanism. As previously mentioned, the grain of matrix metal is much larger in the base metal than that of the bead, and also TiB_2 particles prior to welding presented as larger clusters. α(Al) is very soft but TiB_2 has a very high hardness, which can effectively carry the load. Due to the coarse grain which made the α(Al) expose to the steel counter surface in large area, the base metal shows very poor wear resistance, although the reinforcement phase TiB_2 is distributed in it. In contrast, the matrix metal grains are much smaller and the distribution of TiB_2 particles is much more homogeneous in the welding seam. Due to fine grain strengthening and TiB_2 dispersion strengthening, the wear resistance of weld seam is greatly improved.

4 Conclusions

1) The good defect-free beads are obtained by EB welding under the condition of proper process parameters. The cross-section of welding seam is deep and narrow. Certain scanning rate used in EB welding could prevent porosity successfully. TiB_2 particles presented as clusters in the base metal are separated and distributed much more homogeneously after EB welding.

2) The mechanical properties of welds are superior to the base metal. Fracture occurs in the base metal after tensile tests, and elastic module is also greatly increased compared with pre-welded base metal.

3) Due to the combination of homogeneous particle distribution and fine grain microstructure, the welding seam shows high wear resistance property compared with the base metal.

Acknowledgement

The authors gratefully thank the support of Institute of Ecology and Environmental Materials of Shanghai Jiao Tong University for supplying the materials.

References

[1] ZHANG Yi-jie, JIANG Sheng-ling, MA Nai-heng. The microstructure and properties of in situ TiB_2 particulates reinforced A356 composite [J]. Journal of Shanghai Jiao Tong University: Science, 2007, 41(2): 328−331. (in Chinese)

[2] WANG X H, NIU J T,GUAN S K. Investigation on TIG welding of SiC_p-reinforced aluminum-matrix composite using mixed shielding gas and Al-Si filler [J]. Materials Science and Engineering A, 2009, 499: 106−110.

[3] BASSANI P, CAPELLO E, COLOMBO D. Effect of process parameters on bead properties of A359/SiC MMCs welded by laser [J].Composites A, 2007, 38: 1089−1098.

[4] WANG Shao-gang, XU Jiu-hua, JIANG Cheng-yu. Several technical problems during welding aluminum matrix composites [J]. Aerospace Materials & Technology, 2006, 36(4): 1−6. (in Chinese)

[5] LI Xing-rui, SHI Xin-wei, TANG Wen-bo, WANG Xi-he, NIU Ji-tai. Research processes of SiC_p reinforced Al-matrix composites in arc welding [J]. Hot Working Technology, 2008, 37(9): 95−99. (in Chinese)

[6] GARCIA R, LOPEZ V H, BEDOLLA E, MANZANO A. A comparative study of the MIG welding of Al/TiC composites using direct and indirect electric arc processes [J]. Journal of Materials Science, 2003, 38(12): 2771−2779.

[7] LI Ji-yong, ZHAO Yong, CHEN Hua-bing. Friction stir welding of TiB_2 particulate A356 aluminum alloy composite [J]. Journal of

Materials Engineering, 2005(1): 29−36. (in Chinese)

[8] LIU L M, ZHU M L, NIU J T. Study on the behavior of reinforcement in molten pool for submicron composite Al_2O_{3p}/6061 Al during laser welding [J]. China Welding, 2001, 10(2): 99−103.

[9] NIU Ji-tai, LIU Li-ming, MENG Qing-chang, LIU Xing-qiu. Optimization of welding parameters and microstructure of welded joint of Al_2O_{3P}/6061 Al composite[J]. Transactions of the China Welding Institution, 1999, 20(1): 28−32. (in Chinese)

[10] CUI H C, LU F G, PENG K. Research on electron beam welding of in situ TiB2p /ZL101 composite [J]. Journal of Shanghai Jiao Tong University: Science, 2010, 15(4): 479−483.

[11] JI Xiao-hui, WANG Shao-gang, ZHAO Xiao-qun, DONG Gui-ping. Current research situation of electron beam welding of SiC particulate reinforced aluminum matrix composites [J]. Light Alloy Fabrication Technology, 2009, 37(1): 11−15. (in Chinese)

[12] VINCENT J E, JAMES W K, CHAD M M. Estimation of the thermal conductivity of composites [J]. Journal of Material Science, 1999, 234: 3545−3553.

[13] CUI H C, LU F G, TANG X H, YAO S. Research on laser full-penetration welding in situ TiB_2 particulate reinforced ZL101 composites [J]. Advanced Materials Research, 2010, 97−101: 3967−3973.

[14] HALLUM D L, BAESLACK III W A. Nature of grain refinement in titanium alloy welds by microcooler inoculation [J]. Welding Journal, 1990, 69(9): 326−336.

[15] MA You-peng, XU Yun-hua. Solidification theory and technology [M]. Beijing: Metallurgy Industry Press, 2008: 49−51. (in Chinese)

[16] SCHAFFER P L, MILLER D N, DAHLE A K. Crystallography of engulfed and pushed TiB_2 particles in aluminum [J]. Scripta Materialia, 2007, 57(12): 1129−1132.

[17] ZHAO Hui, HAN Zhong, CHENG Xiao-feng. Effect of scanning electron beam on solidified structure of welded Ti-6Al-4V alloy [J]. Transactions of the China Welding Institution, 2005, 26(1): 78−80. (in Chinese)

[18] ZHANG Wei-ping, LIU Shuo, MA Yu-tao. Strengthening mechanism of particle reinforced metal matrix composite coating by laser cladding [J]. Transactions of Materials and Heat Treatment, 2005, 26(01):70−73. (in Chinese)

电子束焊接铝基复合材料接头的力学性能及耐磨损性能

彭 坤，崔海超，芦凤桂，吴晓敏，唐新华，姚 舜，楼松年

上海交通大学 上海市激光制造与材料改性重点实验室，上海 200240

摘　要：使用装备了可编程序控制器的电子束焊接设备，研究新型铝基复合材料 TiB_2/ZL101 的焊接性。在合适的工艺参数和扫描频率下，通过电子束焊接方法可以得到无缺陷的焊缝，焊后增强相 TiB_2 在焊缝中分布均匀，未出现偏析现象。对焊缝进行拉伸性能测试，均在母材处发生断裂，电子束焊接得到了较高的焊缝强度；通过对焊缝进行磨损测试，焊缝的抗磨损性能得到了显著的提升。研究表明，采用电子束焊接方法可以有效地完成新型铝及复合材料 TiB_2/ZL101 的焊接。

关键词：TiB_2/ZL101 复合材料；电子束焊接；偏析；拉伸；耐磨损

(Edited by LI Xiang-qun)